JOURNAL OF MATERIALS SCIENCE **36** (2001) 3003–3010

Thermal conductivity of dense and porous yttria-stabilized zirconia

K. W. SCHLICHTING*, N. P. PADTURE*, P. G. KLEMENS‡
*Department of Metallurgy and Materials Engineering and ‡Department of Physics, Institute of Materials Science, University of Connecticut, Storrs, CT 06269-3136, USA
E-mail: npadture@mail.ims.uconn.edu

The thermal conductivity of dense and porous yttria-stabilized zirconia (YSZ) ceramics has been measured as a function of temperature in the range 25 to 1000 °C. The dense specimens were either single crystal (8 mol% YSZ) or sintered polycrystalline (3 mol% and 8 mol% YSZ). The porous specimens (3 mol% YSZ) were prepared using the "fugitive" polymer method, where different amounts of polymer spheres (of two different average sizes) were included in the starting powders before sintering. This method yielded materials with uniformly distributed porosities with a tight pore-size distributions. A theory has been developed to describe the thermal conductivity of dense YSZ as a function of temperature. This theory considers the reduction in the intrinsic thermal conductivity due scattering of phonons by point defects (oxygen vacancies and solute) and by the "hopping" of oxygen vacancies. It also considers an increase in the effective thermal conductivity at high temperatures due to radiation. This theory captures the essential features of the observed thermal conductivity. The Maxwell theory has been used to analyze the thermal conductivity of the porous materials. An adequate agreement was found between the theory and experiment.

1. Introduction

Zirconia (ZrO_2) has one of the lowest thermal conductivities in a ceramic, and is, therefore, widely used as thermal insulator at elevated temperatures [1]. One such application of yttria (Y_2O_3)-stabilized zirconia (YSZ) is thermal barrier coatings (TBCs) which are used to protect and insulate hot-section metal components in advanced gas-turbine (aircraft and power generation) and diesel engines (see e.g. review article by Jones [2] and references therein). The use of TBCs can result in a temperature reduction of as much as 200 °C at the metal surface, thereby improving the durability of the metal component and enhancing the engine power-to-weight ratio [3–5]. TBCs, which range in thicknesses from 200–500 μm for gas-turbine engines [5] to 2 mm for diesel engines [6], are deposited onto metallic substrates by the air plasma spray (APS) method. Electron-beam physical vapor deposition (EB-PVD) method is also used, but for relatively thinner (125 to 200 μm), high-performance TBCs [5]. APS coatings contain significant amounts of microstructural defects such as cracks, both parallel (at splats boundaries) and normal to the metal/ceramic interface, and also pores [3]. These defects are deliberately engineered into TBCs, as they impart the system with the much desired quality of strain tolerance, thereby mitigating the stresses due to the thermal-expansion mismatch between the metal and the ceramic [3]. Furthermore, these defects help reduce the thermal conductivity of the TBCs [7].

There have been many studies aimed at understanding the effects of these microstructural defects, porosity in particular, on the thermal conductivity of APS TBCs [7–9]. These studies include thermal conductivity measurements, porosity characterization, and modeling the effect porosity has on thermal conductivity. However, accurate characterization of the porosity in production coatings is very difficult. For example, narrow cracks parallel to the metal/ceramic interface substantially reduce the thermal conductivity, but ordinary porosity measurement methods, such as mercury porosimetry, do not probe these extremely narrow channels. Recently, Dorvaux *et al*. [9] have used image analysis in an attempt to characterize the porosity more accurately. However, a fundamental study of effect of porosity on the thermal conductivity of YSZ is lacking. Also, with a few exceptions, very little effort has gone into the understanding and analysis of the mechanisms of lattice thermal conductivity and radiation in dense YSZ [10–14].

The first objective of this work was to analyze the lattice thermal conductivity of dense YSZ in terms of the various resistive mechanisms. The second objective of this work was to study the effect of porosity on the thermal conductivity of YSZ, where the deliberately

0022–2461

introduced porosity is well-controlled and can be accurately characterized.

2. Experimental procedure

YSZ containing 3 mol% yttria (5.2 wt%) was the primary composition studied. The fugitive-polymer method [15] was used to introduce controlled, spherical porosity in these specimens during sintering. Submicron powder (average particle diameter 0.3 μm and average crystallite size 24 nm) of 3 mol% YSZ were obtained commercially (TZ-3Y, Tosoh Corp., Bound Brook, NJ, USA). A total of 5 different powder batches were prepared by mixing the YSZ powders with polymer spheres (Bangs Laboratories Inc., Fishers, IN, USA) of two different sizes (5.4 and 15.0 μm average diameters) in various volume fractions. Individual powder batches were blended in polyethylene bottles by wet tumbling (without any media) in methanol for 24 h, and each of these slurries were then stirred while drying. Individual pellets (25 mm diameter $\times$ 5 mm thickness) were fabricated by uniaxial pressing of the individual powders batches at a pressure of 50 MPa in a steel die, followed by wet-bag cold-isostatic pressing at 350 MPa. The pressed pellets were then calcined at 1000 °C for 24 h to burnout the polymer spheres, leaving only pores behind, followed by sintering at 1600 °C for 1 h. The same method was also used to fabricate control, dense (>99.9 %) specimens using only as-received YSZ powder without the added polymer spheres.

YSZ containing 8 mol% yttria (13.4 wt%) was used to study the effect of composition on thermal conductivity. Only dense specimens of that composition were fabricated from a commercially available powder (average particle diameter 0.3 μm and average crystallite size 20 nm) of 8 mol% YSZ (TZ-8Y, Tosoh Corp., Bound Brook, NJ, USA), using the above procedure. In order to study the effect of grain boundaries on the thermal conductivity, single crystal specimens of 8 mol% YSZ were obtained commercially (Accumet Materials Co., Ossining, NY, USA). Note that 3 mol% YSZ contains a metastable mixture of monoclinic, tetragonal and cubic phases of ZrO_2, which cannot be prepared in the single crystal form. Thus, a total of 8 types of specimens were studied: 5 porous 3 mol% YSZ, 1 dense 3 mol% YSZ, 1 dense 8 mol% YSZ and 1 single-crystal 8 mol% YSZ.

The density (ρ) of each type of specimen was measured using the Archimedes principle, with water as the immersing medium [16]. Crossection of each type of specimen was also ground and polished to a 1 μm final finish using routine ceramographic methods. Polished cross-sections of the control, dense specimens were thermally etched at 1400 °C for 0.1 h, and their microstructure observed in a scanning electron microscope (SEM, Philips Electron Optics, The Netherlands). These SEM images were scanned into a computer, and the average grain sizes of these specimens were measured using an image analysis software (microGOP 2000, ContextVision, Linköping, Sweden). The average grain size for both compositions was found to be 1.4 μm.

The polished cross-sections of the porous specimens were observed in an optical microscope (METAPHOT, Nikon, Japan). The optical images were recorded, and were also scanned into a computer. The same ContextVision image analysis software was used to measure the pore sizes and the pore volume fractions. About 300 pores per specimen were measured to obtain the average pore size. At least 15 representative micrographs (at 500$\times$ or 1500$\times$ magnification) per specimen were used to obtain pore volume fractions. A stereological factor of 1.27 was used to convert the raw measurements of the pore diameter and the volume fraction to actual values, assuming spherical pores of uniform distribution. This factor accounts for the fact that a random cross-section plane does not, in general, intersect the pores on the diametrical plane.

For each of the aforementioned 8 types of specimens, a set of samples was machined. Each set consisted of a plate sample (12.7 $\times$ 12.7 $\times$ 1.27 mm) and a disk sample (5.8 mm diameter $\times$ 1.52 mm thickness). Thermal diffusivity (κ) of each of the 8 plate samples was measured in the temperature range 23 to 1000 °C during heating (in vacuum) using the laser-flash technique [17]. Because of the translucency of the specimens to the laser, the front face and the back face of the plate specimens were coated with a thin layer of silicon carbide (SiC) and carbon, respectively. Although the carbon coating had no effect on the measurements, appropriate corrections were made in the thermal diffusivity calculations to account for the presence of the silicon carbide layer [18]. Specific heat (c) of each of the 8 disk samples was measured, also in the same temperature range during heating, using differential scanning calorimetry (single-crystal alumina reference material) [17]. The thermal property measurements were performed at the Thermophysical Properties Research Laboratories Inc. (West Lafayette, IN, USA). At a given temperature (T), the thermal conductivity (k) was determined using the relation $k = \kappa\rho c$, where ρ is the density. The thermal conductivity values are accurate within 4%. Some measurements were also performed during cooling. The difference between the respective heating and cooling values was found to be within experimental error.

3. Theoretical analysis

3.1. Dense materials

First we analyze the thermal conductivity of dense YSZ. The total thermal conduction in YSZ can be thought as the sum of contributions from phonons and photons (radiation) [19]:

$$k = k_{\mathrm{P}} + k_{\mathrm{R}}. \tag{1}$$

The phonon thermal conductivity of a pure solid, in the absence of any extrinsic scattering by extended defects (grain boundaries, pores) or point defects (vacancies, solute atoms), is simply [19]:

$$k_{\mathrm{P}} = k_{\mathrm{Intrinsic}} = \frac{\psi}{T}, \tag{2a}$$

where T is the absolute temperature of interest and ψ is a constant and is given by [19]:

$$\psi = \frac{3}{2}\gamma^2\left[\frac{\mu\nu^2}{\omega_D N^{-2/3}}\right], \quad (2b)$$

with γ being the Grüneisen parameter which is a measure of the anharmonicity, μ being the shear modulus, ν being the transverse phonon velocity (which is $(\mu/\rho)^{1/2}$ with ρ being the density), ω_D being the Debye frequency, and N being the number of atoms in the molecular-formula unit of the solid. Many of these properties for pure zirconia are not known because single-crystal or polycrystalline unstabilized zirconia specimens cannot be fabricated. Thus, the value of ψ zirconia has been estimated to vary between 1,700 and 2,800 Wm^{-1} [12, 13], and can be treated as an adjustable parameter. (Note that the value of ψ for single-crystal titania (TiO_2) has been determined to be 2,800 Wm^{-1} [20].)

With the addition of yttria, the phonons can be scattered by the oxygen vacancies that are created. Thus, the phonon conductivity now becomes [21]:

$$k_P = \left[\frac{\psi}{T}\right](\omega_O/\omega_M)\tan^{-1}(\omega_M/\omega_O) \quad (3a)$$

with

$$(\omega_O/\omega_M)^2 = \frac{\chi T}{\{C(1-C)\}}, \quad (3b)$$

where ω_M is the phonon frequency corresponding to the maximum of the acoustic branch of the phonon spectrum, ω_O is that phonon frequency where the intrinsic mean free path is equal to that due to solute atoms, C is the fractional molar concentration of yttria, and χ is a constant with a value of 9.82×10^{-3} for YSZ [13]. Since the grain size of the YSZ in question is fairly large (1.4 μm), we do not expect significant reduction by phonon scattering from grain boundaries [13]. This assumption will be validated experimentally in Section 4.

The phonon conductivity can be further reduced by the scattering of phonons due to the jumping of oxygen vacancies between neighboring sites in the lattice. This mechanism is dominant at temperature below 100 °C and the reduction in thermal conductivity takes the form [13]:

$$\Delta k_{Hopping} = \frac{k_{Intrinsic}\xi}{T} = \frac{\psi\xi}{T^2}, \quad (4)$$

where ξ is a constant, which can be deduced from measurements of the thermal conductivity at low temperatures assuming that the same mechanism operates above room temperatures. Thus, from measurements on YSZ one expects ξ to lie between 40 and 50 K, and can be treated as an adjustable parameter [13]. The reduction given by Equation 4 is due to scattering of phonons at low frequencies, and is independent of the reduction due to point defects, which scatter phonons in a different, high frequency range.

The phonon conductivity, considering the three scattering mechanisms of (i) intrinsic scattering due to the interaction between phonons owing to lattice anharmonicity, (ii) scattering due to oxygen vacancies, and (iii) scattering due to oxygen vacancy jumping, is then given by [22]:

$$k_P = \left\{\left[\frac{\psi}{T}\right](\omega_O/\omega_M)\tan^{-1}(\omega_O/\omega_M)\right\} - \left[\frac{\psi\xi}{T^2}\right]. \quad (5)$$

Heat can also be transferred by radiation or by photons, a mechanism that is dominant at elevated temperatures. However, radiation is effective only in a narrow window of frequency. Below the absorption edge f_A, radiation is not transmitted. Similarly, above a very high frequency f_O, radiation is strongly scattered. The effective thermal conductivity due to radiation is then given by [19]:

$$k_R = \left[\frac{4\sigma\varepsilon L n^2 T^3}{25.976}\right]\{J_4(\Theta_O/T) - J_4(\Theta_A/T)\}, \quad (6a)$$

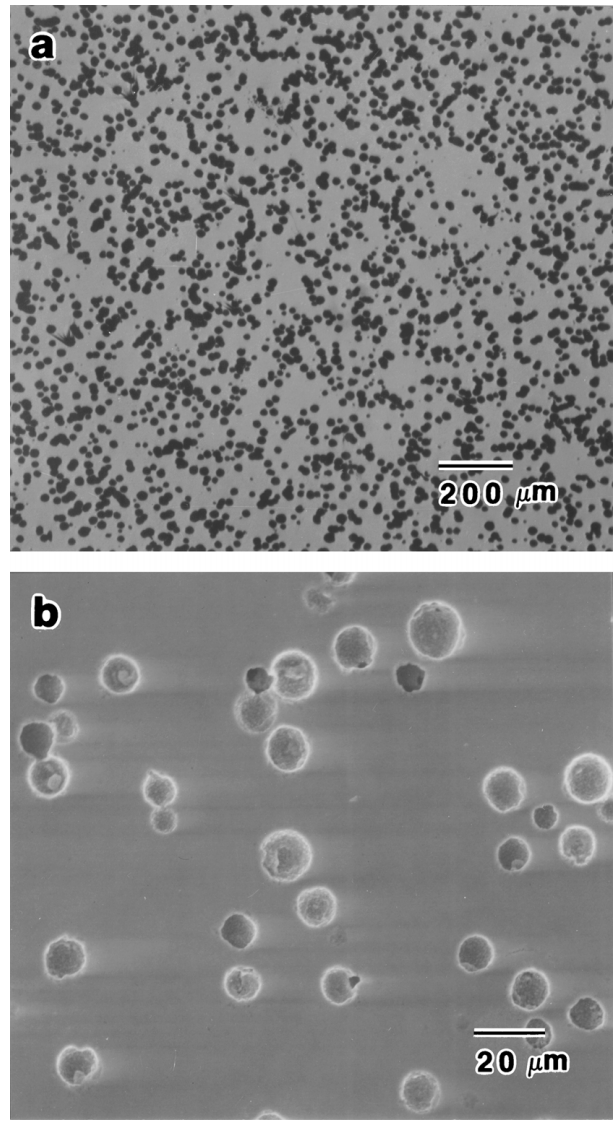

Figure 1 (A) Representative optical micrograph showing the uniform distribution of the porosity. (B) A close-up scanning electron micrograph showing the spherical shape of the pores. 3 mol% YSZ specimen with 9.9% porosity and average pore size 14.9 μm.

where the J_4 function is defined as [23]:

$$J_4(\Theta/T) = \int_0^{(\Theta/T)} \{(x^4 e^x)/(e^x - 1)^2\}\, dx, \qquad (6b)$$

and σ is the Stefan-Boltzmann constant, ε is the effective emissivity (recall that the plate specimen is bounded by silicon carbide on one face and carbon on the other), L is the thickness of the plate across which radiation is occurring (recall that $L = 1.27$ mm in our experiments), and n is the refractive index ($= 2.7$ for YSZ [24]). The variables $\Theta_O = hf_O/k_B$ and $\Theta_A = hf_A/k_B$, where h and k_B are the Planck and Boltzmann constants, respectively. For very high frequencies Θ_O approaches infinity, resulting in $J_4(\Theta_O/T) = 25.976$ [23]. Since the absorption edge, f_A, for YSZ occurs at 6×10^{13} Hz [24], Θ_A is 2900 K. The function J_4 has been tabulated [23], being the same as it occur in the

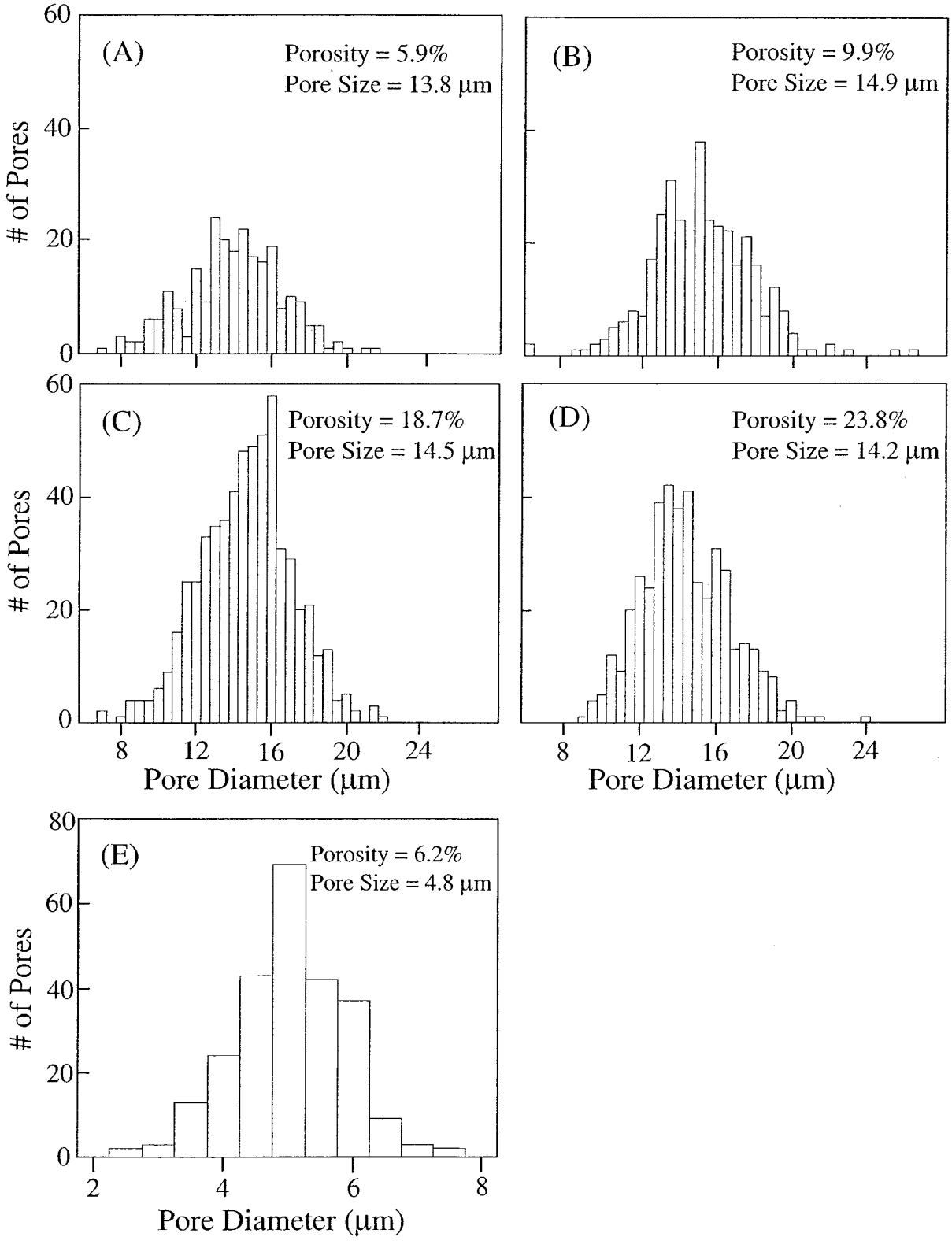

Figure 2 Histograms showing pore size distributions in the porous YSZ specimens.

Debye theory of specific heat. The effective emissivity ε is not well known. In our case it is the emissivity between zirconia and silicon carbide, and is treated as an adjustable parameter.

Once again, the total thermal conductivity is given by the sum of the phonon and the photon contributions (Equation 1).

3.2. Porous materials

There is an extensive but scattered literature dealing with the effect of inclusions and pores on the electrical and thermal conductivities and dielectric constant. For thermal conductivity there is a valuable discussion in a book by Parrott and Stuckes [25]. They point out that the overall conductivity cannot exceed the volume average of the components, and cannot be above the value obtained from the volume average of the resistivities. In the case of pores in solids the second limit is not useful, since pores have almost infinite resistivity.

First, we consider the reduction in the phonon thermal conductivity (k_P) due to porosity. An early theoretical treatment was given by Maxwell [26], where he calculated the current lines around a spherical inclusion in a cube of unit volume for inclusion volume fraction of ϕ. He showed that [26]:

$$\frac{k_{\text{Mixture}}}{k_P} = \frac{[1 + 2\delta - 2\phi(\delta - 1)]}{[1 + 2\delta + \phi(\delta - 1)]}, \tag{7}$$

where k_{Mixture} is the effective conductivity of the mixture, k_P is the phonon conductivity of the continuous phase, $\delta = k_P/k_{\text{Inclusion}}$, and $k_{\text{Inclusion}}$ is the conductivity of the inclusion. In the case of pores $\delta \to \infty$, and one obtains for the phonon conductivity ratio:

$$\frac{k_{\text{P(Porous)}}}{k_{\text{P(Dense)}}} \approx 1 - \frac{3}{2}\phi. \tag{8}$$

There are other approximations, including that by one of us [27], where the spatial variation about the volume average of the conductivity is expressed in Fourier components, as is the field, and the field components are adjusted to minimize the rate of entropy production. The resulting set of equations can be solved by iteration. For pores, where $k_{\text{Inclusion}} = 0$, we have [27]:

$$\frac{k_{\text{P(Porous)}}}{k_{\text{P(Dense)}}} = 1 - \frac{4}{3}\phi. \tag{9}$$

Equation 9 was previously used by us for the analysis of the phonon conductivity of porous YSZ [28].

Now, we consider the reduction in the photon thermal conductivity (k_R) due to porosity. At elevated temperatures, the presence of pores reduces the dielectric constant (n^2) of the material, which appears as a multiplicative factor in the expression for the radiative component (k_R; Equation 6). An additional reduction in k_R can occur due to pore-scattering. However, since the average pore sizes (5 and 14 μm) of the materials studied here are much larger than the radiation wavelengths, the scattering is expected to be negligible.

In an inhomogeneous medium, the effective value of n^2, and thus k_R (Equation 6), is given by similar considerations as the effective conductivity, since displacement fields and current lines are governed by the same equation. In the case of pores, for which $n^2_{\text{Inclusion}} = 1$ and $\delta = n^2_{\text{Dense}}$, Maxwell's expression (Equation 8), for small ϕ, becomes [26]:

$$\frac{k_{\text{R(Porous)}}}{k_{\text{R(Dense)}}} \approx 1 - \frac{3}{2}\phi\frac{n^2_{\text{Dense}} - 1}{n^2_{\text{Dense}} + \frac{1}{2}}. \tag{10}$$

Note that this ratio is always smaller than the corresponding ratio in Equation 8, by a factor of $\approx$0.81 for $n^2_{\text{Dense}} = 2.7$ for YSZ. Similarly, for relation by Klemens [27] (Equation 9), one obtains:

$$\frac{k_{\text{R(Porous)}}}{k_{\text{R(Dense)}}} \approx 1 - \phi\frac{n^2_{\text{Dense}} - 1}{n^2_{\text{Dense}}}\left[1 + \frac{1}{3}\frac{n^2_{\text{Dense}} - 1}{n^2_{\text{Dense}}}\right]. \tag{11}$$

Once again, this ratio is smaller than that given by Equation 9, here by a factor of $\approx$0.83.

Since the extra factors in Equations 10 and 11 for radiation are expected to have a negligible effect, it is expedient to use the following relation due to Maxwell for the relative overall thermal conductivity of porous materials ($k_{\text{porous}} = k_{\text{P(Porous)}} + k_{\text{R(Porous)}}$; Equation 1) [26]:

$$\frac{k_{\text{Porous}}}{k_{\text{Dense}}} = 1 - \frac{3}{2}\phi, \tag{12}$$

or the one due to Klemens [27]:

$$\frac{k_{\text{Porous}}}{k_{\text{Dense}}} = 1 - \frac{4}{3}\phi. \tag{13}$$

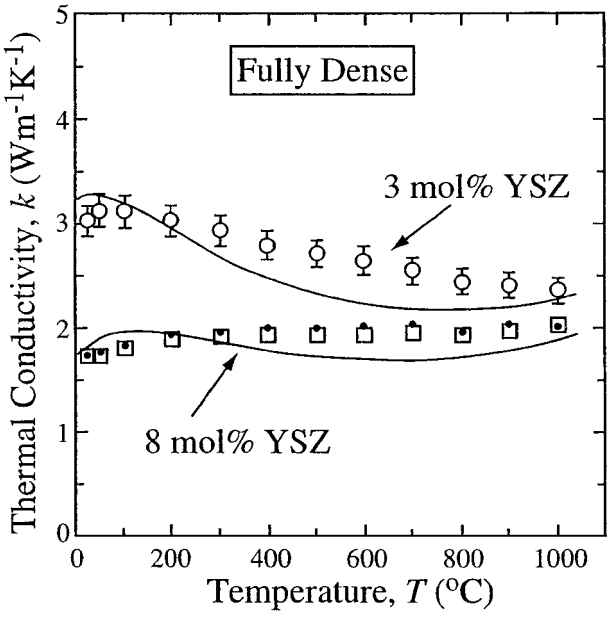

Figure 3 Thermal conductivity of fully dense YSZ specimens as a function of temperature. Open symbols represent polycrystalline specimens and filled dots (•) represent data for the 8 mol% YSZ single crystal specimen. Error bars smaller than symbol size not shown. Solid lines represent the theoretical fits (Equations 1–6) to the data.

TABLE I Characteristics of the 8 specimens used in this study

Composition	Type	Specimen Number	Average Pore Diameter (μm)	Volume% Porosity	Density (Mg/m^3)
3 mol% YSZ	Dense	1	-	-	6.086
	Porous	2	4.8	6.2	5.777
		3	13.8	5.9	5.733
		4	14.9	9.9	5.532
		5	14.5	18.7	4.973
		6	14.2	23.8	4.664
8 mol% YSZ	Dense	7	-	-	5.938
	Single Crystal	8	-	-	5.968

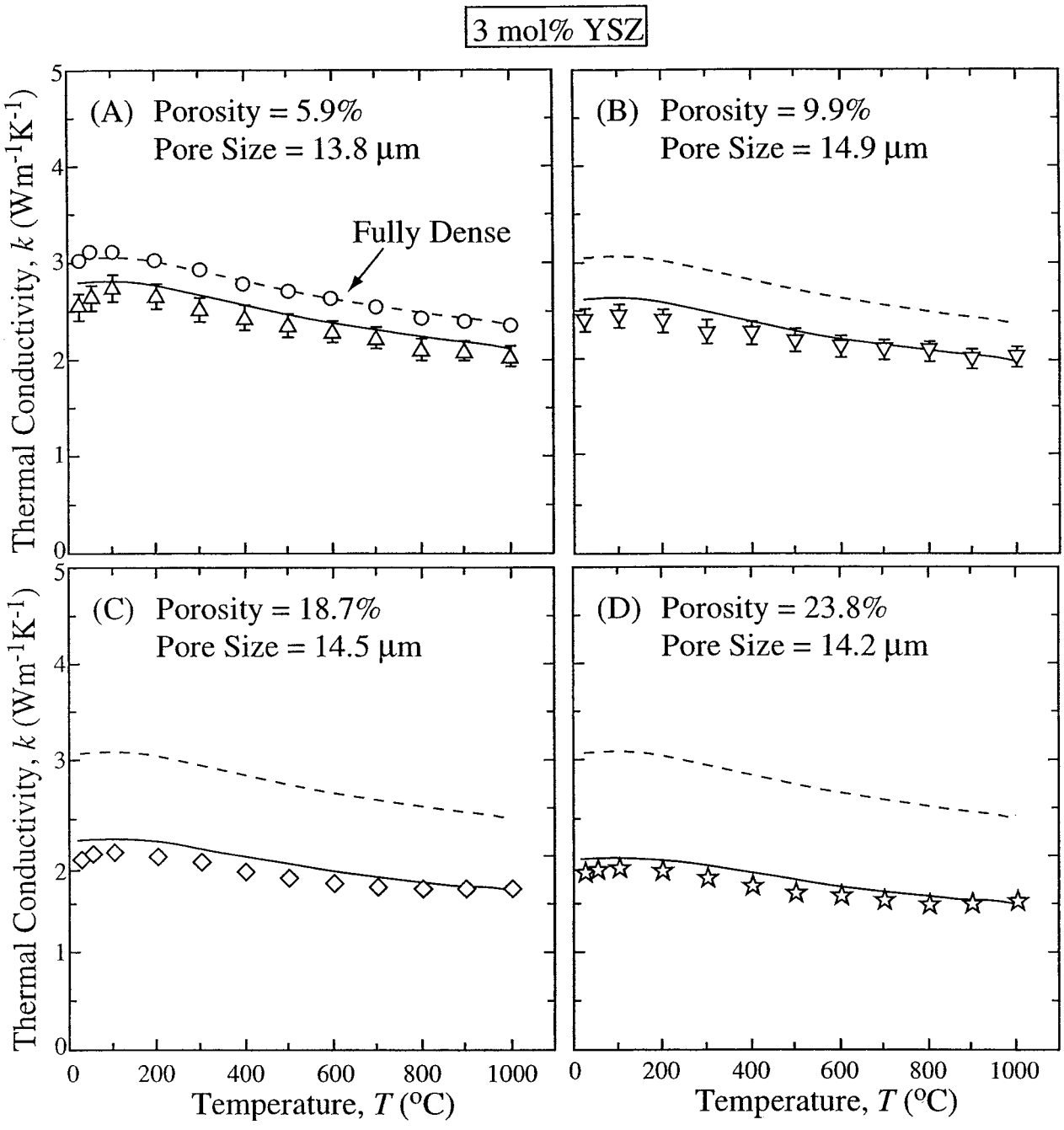

Figure 4 Thermal conductivity of porous 3 mol% YSZ specimens as a function of temperature. Error bars smaller than symbol size (except fully dense specimen) not shown. Dashed line represents an empirical fit to the data for the fully-dense specimen. Solid lines represent theoretical fit (Equation 12) to the data.

to analyze the effect of porosity (ϕ) on the thermal conductivity of YSZ.

4. Results and discussion

Fig. 1A and 1B show microstructure of a porous specimen at different magnifications. Note the near-spherical shape of the pores and the uniform distribution of the pores throughout the specimen. These features were observed to be typical of all the porous specimens studied. Fig. 2A through 2E show pore size distributions for the 5 porous specimens. Table I summarizes the characteristics of the 8 specimens used in this study.

Fig. 3 shows the thermal conductivity as a function of temperature for the dense specimens and the single crystal specimen. For the dense 3 mol% YSZ specimen note the modest temperature dependence, which is typical of zirconia ceramics. For the dense 8 mol% YSZ specimen that independence is more pronounced, with the thermal conductivity showing a slight increase with temperature. Note the identical thermal conductivities for both single-crystal and polycrystalline 8 mol% YSZ, confirming the lack of the effect of grain boundaries on the thermal conductivity in the temperature range studied.

The solid lines in Fig. 3 represent predictions from the theory described in Section 3 (Equations 1–6). The following values for the adjustable parameters were used to obtain a good fit: $\psi = 2{,}700\ \mathrm{Wm}^{-1}$, $\xi = 50$ K, and $\varepsilon = 0.136$. Once again, these values are reasonable estimates, as independent measurement of these parameters is an intractable task. Note the fit between the theory and the experiment at the extremes of the temperature range, and the discrepancy at intermediate temperatures, which is more pronounced in the case of 3 mol% YSZ. The maximum discrepancy in the intermediate temperatures is observed to occur near 650 °C for 3 mol% YSZ. This is possibly due to the combination of an overestimation of phonon scattering (steeper temperature dependence) and an underestimation of the radiative component. However, since that fit appears to be better in the case of 8 mol% YSZ and since the radiative component is independent of the yttria concentration (Equation 6), it is argued that the discrepancy may be due to a larger overestimation of the phonon scattering in the case of 3 mol% YSZ relative to 8 mol% YSZ. In other words, there may be additional scattering centers or mechanisms, other than the compensating point defects, in 3 mol% YSZ which have not been accounted for. At this time it is not clear what those centers or mechanisms may be.

In Fig. 3, also note that the theory captures the downturn observed in the low-temperature thermal conductivity data. That downturn in the theoretical curves is due to the phonon-scattering by oxygen-vacancy hopping (Equation 4). Note that the downturn occurs at a lower temperature in 3 mol% YSZ relative to 8 mol% YSZ. This is consistent with the fact that there are relatively fewer oxygen vacancies in the 3 mol% YSZ material.

Fig. 4A to 4D show the effect of porosity on the thermal conductivity of 3 mol% YSZ. The dashed line represents an empirical fit through the data for the fully dense material. The solid lines for the porous materials are theoretical fits using the Maxwell [26] relation (Equation 12). The baseline thermal conductivity for the dense material (dashed line) was used as k_{Dense} in Equation 12. There is an adequate agreement between the theory and the experiment (within 8% overall). Recall that the error in the measurement was estimated at about 5%. The Klemens [27] relation (Equation 13) was also used to fit the experimental data (not shown here), but it did not yield as good a fit (over 10% error overall). Note that the relation due to Klemens [27] (Equation 13) assumes no correlation in the position of the pores, while that due to Maxwell [26] (Equation 12) assumes well separated pores. Since the pores in the YSZ materials studied here were formed from solid polymer spheres which cannot overlap, the Maxwell [26] relation is expected to yield a better correlation in analyzing the thermal conductivity data for porous YSZ. Also, note that the porosity effect is expected to be independent of the pores size (Equations 12 and 13), since the sizes of the pores are much larger than the wavelength of the radiation and are not expected to scatter radiation to a significant extent. This is confirmed in Fig. 5, which plots the thermal conductivity data for YSZ specimens containing 2 different average pores sizes (4.8 and 13.8 μm) but the same amount of porosity (~6%).

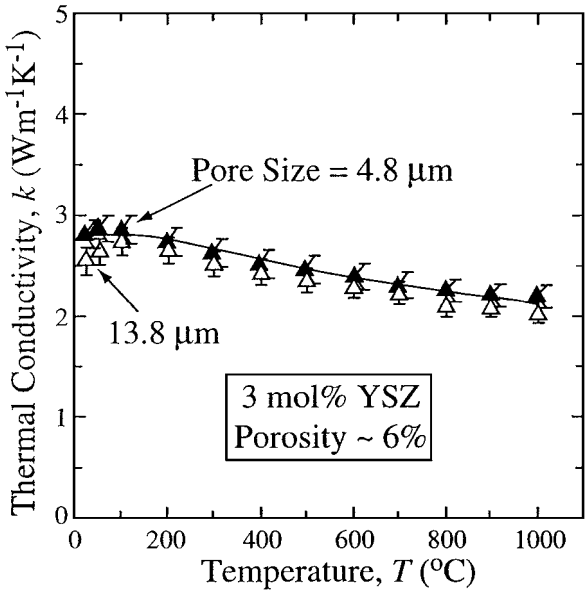

Figure 5 Thermal conductivity as a function of temperature for porous 3 mol% YSZ specimens with 2 different average pore sizes (4.8 and 13.8 μm) but the same porosity (~6%).

5. Summary

We have measured the thermal conductivity of dense and porous yttria-stabilized zirconia (YSZ) ceramics as a function of temperature in the range 25 to 1000 °C. The dense specimens were either single crystal (8 mol% YSZ) obtained commercially or in-house sintered polycrystalline (3 mol% and 8 mol% YSZ). The porous specimens (3 mol% YSZ) were prepared using the "fugitive" polymer method, where different amounts of

polymer spheres (of two different average sizes) were included in the starting powders before sintering. This method yielded materials with uniformly distributed porosities with a tight pore-size distributions. As reported by others, the overall thermal conductivity of YSZ is not a strong function of temperature. A theory was developed to describe the thermal conductivity of dense YSZ as a function of temperature. This theory considers the reduction in the intrinsic thermal conductivity due scattering of phonons by point defects (oxygen vacancies and solute) and by the "hopping" of oxygen vacancies. It also considers an increase in the effective thermal conductivity at high temperatures due to radiation. This theory was found to capture the essential features of the observed thermal conductivity. However, there was a poor agreement between theory and experiment in the intermediate temperature range, especially in the case of 3 mol% YSZ, the reason for which is not clear at this time. The Maxwell theory was used to analyze the thermal conductivity of the porous materials, where an adequate agreement was found between theory and experiment.

Acknowledgement

The authors thank Profs. M. Gell and E. H. Jordan (University of Connecticut) for many fruitful discussions, and Dr. R. E. Taylor (TPRL Inc.) for performing the thermal conductivity measurements. Financial support for this work was provided by the Office of Naval Research (Contract No. N00014-97-1-0843).

References

1. W. D. KINGERY, H. K. BOWEN and D. R. UHLMANN, "Introduction to Ceramics" (Wiley Interscience, New York, 1976).
2. R. L. JONES, in "Metallurgical and Ceramic Coatings," edited by K. H. Stern (Chapman & Hall, London, 1996) p. 194.
3. R. J. BRATTON and S. K. LAU, in "Advances in Ceramics: Science and Technology of Zirconia," Vol. 3, edited by A. H. Heuer and L. W. Hobbs (The American Ceramic Society, Columbus, OH, USA, 1981) p. 226.
4. K. D. SHEFFLER and D. K. GUPTA, *J. Eng. Gas Turbines and Power (Trans. ASME)***110** (1988) 605.
5. S. M. MEIER, D. K. GUPTA and K. D. SHEFFLER, *J. Metals* **43** (1991) 50.
6. R. C. NOVAK, A. P. MATARESE, R. P. HUSTON, A. J. SCHARMAN and T. M. YONUSHONIS, *Mater. Manuf. Processes* **7** (1992) 15.
7. H. E. EATON, J. R. LINSEY and R. B. DINWIDDIE, in "Thermal Conductivity 22," edited by T. W. Tong (Technomic, Lancaster, PA, USA, 1994) p. 289.
8. R. MCPHEARSON, *Thin Solid Films* **112** (1984) 89.
9. J.-M. DORVAUX, O. LAVIGNE, R. MEVREL, M. POULAIN, Y. RENOLLET and C. RIO, in Proceedings of the 85th Meeting of the AGARD Structures and Materials Panel, Neuilly-sur-Seine, France, 1998, Vol. R-823, edited NATO and AGARD, p. 13.
10. D. P. H. HASSELMAN, L. F. JOHNSON, L. D. BENTSEN, R. SYED, H. L. LEE and M. V. SWAIN, *Am. Ceram. Soc. Bull.* **66** (1987) 799.
11. G. E. YOUNGBLOOD, R. W. RICE and R. P. INGEL, *J. Amer. Ceram. Soc.* **71**(4) (1988) 255.
12. S. RAGHAVAN, H. WANG, R. B. DINWIDDIE, W. D. PORTER and M. J. MAYO, *Scripta Mater.* **39**(8) (1998) 1119.
13. P. G. KLEMENS, in "Thermal Conductivity 23," edited by K. E. Wils, R. B. Dinwiddie and R. S. Graves (Technomics Publishing Co., Lancaster, PA, USA, 1996) p. 209.
14. *Idem.*, in "Chemistry and Physics of Nanostructures and Related Non-Equilibrium Materials," edited by E. Ma, B. Fultz, R. Shull, J. E. Morral and P. Nash (TMS, Warrendale, PA, USA, 1997) p. 87.
15. J. ZHAO and M. P. HARMER, *J. Amer. Ceram . Soc.* **70** (1988) 449.
16. E. C. M. PENNINGS and W. GRELLNER, *ibid.* **72** (1989) 1268.
17. R. E. TAYLOR and K. D. MAGLIC, in "Compendium of Thermophysical Property Measurement Methods," Vol. 1, edited by K. D. Maglic, A. Cezairliyan and V. E. Peletsky (Plenum Press, New York, NY, USA) 1984.
18. K. D. MAGLIC and R. E. TAYLOR, in "Compendium of Thermophysical Property Measurement Methods," Vol. 2, edited by K. D. Maglic, A. Cezairliyan and V. E. Peletsky (Plenum Press, New York, NY, USA) 1992.
19. P. G. KLEMENS, in "Thermal Conductivity," Vol. 1, edited by R. P. Tyne (Academic Press, London, UK, 1969) p. 1.
20. Y. S. TOULOUKIAN, R. W. POWELL, C. Y. HO and P. G. KLEMENS, "Thermophysical Properties of Matter: Vol. 2, Thermal Conductivity" (Plenum, New York, NY, USA, 1970).
21. P. G. KLEMENS, *Phys. Rev.* **119** (1960) 507.
22. *Idem.*, *Physica B* **263-264** (1999) 102.
23. W. M. ROGERS and R. L. POWELL, *NBS Circular* **595** (1958) 1.
24. D. L. WOOD and K. NASSAU, *Applied Optics* **21** (1982) 2978.
25. J. E. PARROTT and A. D. STUCKES, "Thermal Conductivity of Solids" (Pion Ltd., London, UK, 1975).
26. J. C. MAXWELL, "A Treatise on Electricity and Magnetism" (Clarendon Press, Oxford, UK, 1904).
27. P. G. KLEMENS, *High Temps.-High Press.* **23** (1991) 241.
28. K. W. SCHLICHTING, N. P. PADTURE and P. G. KLEMENS, in "Thermal Conductivity 25," edited by C. Uher and D. Morelli (Technomic, Lancaster, PA, USA, 2000) p. 162.

Received 28 March
and accepted 26 December 2000